

CrossMark
click for updatesCite this: *J. Mater. Chem. A*, 2015, 3,
1795

Potential of metal-free “graphene alloy” as electrocatalysts for oxygen reduction reaction

Dongsheng Geng,^a Ning Ding,^a T. S. Andy Hor,^{ab} Zhaolin Liu,^{*a} Xueliang Sun^{*c}
and Yun Zong^{*a}

Extensive research and development on theoretical calculation and synthetic methods over the past few years have made doped graphene one of the most promising candidates for metal-free oxygen reduction reaction (ORR) catalysts. However, from the performance point of view, there is still a long way to go for these doped graphene-based catalysts to meet the requirements needed for commercial applications. What is the key to further improve the catalytic activity of doped graphene toward ORR to make them commercially viable? In this review, we will try to answer this question by fundamentally giving a detailed analysis based on the theoretical calculations to reveal the origin of ORR activity of doped graphene and the structure–performance relationship of such materials. Thereafter, we will provide an overview on the recent advances in the catalytic activity improvement of doped graphene, including major works using approaches of increasing the number of active sites, controlling the doping types (particularly for nitrogen doped graphene), developing co-doped graphene, and extending the surface area of doped graphene. Finally, in this perspective, we discuss some development opportunities and pathways that can lead to more efficient doped-graphene based ORR electrocatalysts approaching the practical use for fuel cells and metal–air batteries.

Received 21st November 2014
Accepted 24th November 2014

DOI: 10.1039/c4ta06008c

www.rsc.org/MaterialsA

1. Introduction

Oxygen reduction reaction (ORR) is one of the most important electrocatalytic reactions because of its critical role in electrochemical energy conversion (*e.g.* fuel cells, metal–air batteries, *etc.*), corrosion (and corrosion inhibition), and a few other industrial processes. The application of ORR in fuel cells has always been the research focus area of material chemists and electrochemists in the past few decades. Polymer electrolyte membrane fuel cells (PEMFCs), ecologically friendly devices that directly convert chemical energy into electricity with high efficiency, are considered to be one of the most promising energy-conversion technologies available.¹ In a fuel cell, the fuel (such as hydrogen, methanol, and formic acid) is oxidized at the anode, and the released electrons are transferred to cathode where oxygen is reduced. Generally, ORR at the cathode has sluggish reaction kinetics, which limits the cell performance. To maintain the cell operation, a large amount of platinum is required in the form of nanoparticles to catalyze the ORR. Pt nanoparticles supported on high surface area carbon (Pt/C)

have long been regarded as the best catalyst for ORR; however, their prohibitive cost, limited resources and insufficient durability preclude the commercial viability of fuel cell technology using such catalyst, despite the successful demonstration of alkaline fuel cells with platinum as an electrocatalyst in the Apollo lunar mission in the 1960s.² The key technological breakthrough to look forward to the broad applications of fuel cells will be catalysts that are capable of efficiently accelerating the ORR yet possesses enhanced stabilities at low cost.^{3,4} Over the past years, considerable effort has been devoted to the development of alternative ORR electrocatalysts with improved activity and stability, which has been systematically reviewed previously.^{5–7} To summarize, there are two main categories of such electrocatalysts as shown in Table 1: (i) modifying Pt/C catalyst *via* alloying approach,^{8–11} constructing nanostructures^{12–17} or replacing conventional carbon black support;^{18–21} (ii) replacing Pt-based catalysts with Pt-free, non-precious metal catalyst, or even non-metal catalysts.^{22–32}

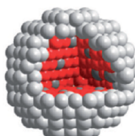
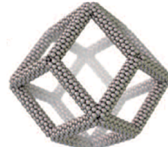
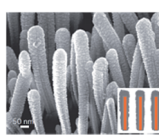
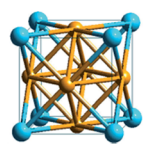
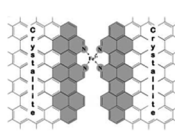
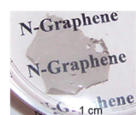
Although considerable progress has been made in modifying Pt/C catalyst, none of the strategies has sufficiently addressed the cost issue owing to the demand and price fluctuation of platinum. Thus, considerable attentions are drawn to non-metal catalysts (doped carbon materials) – inherently cheap and abundant materials. Ozkan *et al.* reported ORR active nitrogen-containing carbon nanostructures, CN_x.^{33–35} Gong *et al.* grew nitrogen doped carbon nanotubes as vertically aligned arrays, which catalyze the ORR in highly alkaline solutions with

^aInstitute of Materials Research and Engineering (IMRE), A*STAR (Agency for Science, Technology and Research), 3 Research Link, Singapore 117602, Singapore. E-mail: zl-liu@imre.a-star.edu.sg; y-zong@imre.a-star.edu.sg

^bDepartment of Chemistry, National University of Singapore, 3 Science Drive 3, Singapore 117543, Singapore

^cDepartment of Mechanical and Materials Engineering, University of Western Ontario, 1151 Richmond Street N., London, Canada. E-mail: xsun@eng.uwo.ca

Table 1 Progress in the development of ORR electrocatalysts. (a) Core-shell bimetallic nanoparticles from electrochemical dealloying. Red and light-grey spheres denote Cu and Pt atoms, respectively, reproduced with permission.¹¹ Copyright 2011, American Chemical Society. (b) Schematic illustration of Pt₃Ni nanoframes with Pt-skin surfaces; reprinted with permission.¹⁷ Copyright 2014, American Association for the Advancement of Science (AAAS). (c) HRSEM of a group of whiskers made of aligned perylene red coated by Pt-based metal thin film; reprinted with permission.¹⁸ Copyright 2012, Macmillan Publishers Ltd. (d) The possible structure of PdCu, reproduced with permission.³¹ Copyright 2014, American Chemical Society. (e) The plat view of presumed active site of Fe-based non-precious metal catalyst; reprinted with permission.²⁵ Copyright 2009, American Association for the Advancement of Science (AAAS). (f) A digital photo image of transparent N-graphene film, reproduced with permission.³² Copyright 2010, American Chemical Society

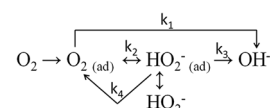
Category	Modifying Pt/C			Replacing Pt/C		
	Alloying	Nanostructured Pt	Novel supports	Pd-based catalyst	Non-precious metal catalyst	Metal-free catalyst
Featured examples						

activities comparable to that of platinum.³⁶ With graphene being introduced as a new type of carbon material in recent years, this 2D material comprising single planar sheet of carbon atoms (sp² bonded) located along the corner of a hexagon has come into the central stage of various research areas. Pristine graphene exhibits unique electronic, optical, thermal, chemical, and mechanical properties that are distinct from other forms of carbon.^{37,38} Ever since its discovery, the possibility of introducing hetero-atoms into graphene lattices opens up the opportunities for the development of new materials with similar morphology but distinct chemical composition and catalytic behavior.^{39–41} To date, heteroatoms, such as B, N, S, P, F, I, and Se, have been introduced into graphene by single, or binary even ternary doping, leading to the formation of “graphene-alloy”, a new type of 2D material, which ensemble graphene but with part of the carbon atoms replaced by one or more types of heteroatoms and thus presenting enhanced electrocatalytic activity toward oxygen reduction.^{32,42–83} Concurrently, theoretical study has demonstrated that doping with foreign atoms is a feasible way to tune the chemical and electronic structure of graphene, which in turn enhances its catalytic activity.^{84–109} Development of doped graphene (or graphene alloy) as metal-free ORR electrocatalyst has thus become a foremost subject in the study of oxygen reduction reactions.^{110–119} A number of research groups have extensively reviewed the synthesis and electrochemical properties of doped graphene;^{120–128} however, a comprehensive overview on the active sites of doped graphene and their role in ORR is absent. To be up to date with the rapid advances in this field, it is time to review the efforts in the identification of real active center of doped graphene and the understandings on their ORR mechanism, which are the prerequisites of designing doped graphene electrocatalyst with further improved ORR activity. In this review, we start with the fundamentals in the doped graphene electrocatalyst development in order to answer the following questions: (i) why is doped graphene active toward ORR? (ii) What is the ORR

mechanism on doped graphene? (iii) What is the real active center of doped graphene for ORR? Based on these understandings, we represent the latest advances in design of doped graphene materials. The review is concluded with prospects and opportunities for future research in this field.

2. Mechanism aspects of oxygen reduction by doped graphene

Generally, doped graphene shows comparable electrocatalytic properties with Pt only in alkaline electrolyte. Thus, unless otherwise stated, the ORR activities of doped graphene mentioned in this review are tested in alkaline electrolytes. Due to its sluggish reaction kinetics the ORR process is rather complicated, involving many intermediates, electron transfer and possible multiple chemical reaction steps, depending on the natures of the catalysts and electrolytes.^{129–132} There is no unanimous consensus on the intermediate formation and the involved reactive species, and the exact mechanism remains unknown. However, the principal ORR process on Pt surface is well accepted and is depicted by Scheme 1, which also works for most of other ORR catalysts, including doped graphene.¹³³ As shown, ORR takes place mainly *via* two overall pathways: one is a “direct” four-electron reduction of O₂ to OH[−], and the other is a “peroxide” pathway, which involves HO₂[−] as the intermediate. The former is desirable for a catalyst, as by which a larger current density and higher onset potential (0.401 V for 4 e[−] pathway *vs.* −0.065 V for 2 e[−] pathway) are delivered.^{134,135}



Scheme 1 Scheme of the ORR on Pt surface in alkaline environment, reproduced with permission.¹³³ Copyright 2002, Elsevier B.V.

However, the high overpotential for the four-electron reduction of oxygen remains the bottleneck of the electrocatalyst development. This is because during the course of overall reaction process any exergonic reaction will contribute to the overpotential. Hence, the most basic requirement for a good candidate of ORR electrocatalyst to possess is that it should bind O_2 weakly (lowest possible adsorption energy for the first step in Scheme 1) to avoid loss due to unnecessarily high energy barriers at later steps toward hydroxyl ion (water) formation.

Boukhalov *et al.* studied the ORR on pure and nitrogen-doped graphene using a first-principles modeling.⁹⁴ They proposed that oxygen forms an ionic bond with N-doped graphene with a “bond-length” of ~ 2.30 Å, which is smaller than the graphene–oxygen “bond-length”. As a result, the energy cost of oxygen adsorption step is lower for doped graphene than that for pristine graphene. Okamoto calculated the O_2 adsorption energy on graphene and N-doped graphene using density-functional theory (DFT).⁹² Their results show that the endothermicity of O_2 adsorption on the N-doped graphene sheet lowers as the number of N in their model increases. The adsorption behavior inverses and becomes exothermic as the number of N atoms becomes sufficiently large. This suggests a decreased repulsive interaction between an O_2 and N-doped graphene sheet (compared to pristine graphene sheets), which is probably benefitted from the charge-transfer. Kabayashi’s study arrived at the conclusion that nitrogen substitution enhances binding interactions of graphene with O_2 molecule due to higher spin density and hybridization freedom of C atoms.⁹⁶ Ikeda *et al.* checked possible oxygen adsorption on the exposed edges of nitrogen doped graphene catalysts using various models, in which the results showed that the O_2 adsorption depends on the morphology and the atomic structure of the system. They claimed that only N in zigzag edges play a critical role in reducing free-energy barrier for O_2 adsorption,⁸⁶ which is in good accordance with the observation of Bao *et al.*⁹¹ They also made a comparison between the chemisorption of O_2 on the edges and on interior sites of graphene doped with quaternary-N, and concluded that the quaternary-N atom doped at the zigzag edge is more favorable for O_2 adsorption, giving the exothermic edge adsorption energy of -18.5 kcal mol⁻¹ through the “two-feet” adsorption fashion (the mode of adsorption will be further discussed in the next paragraph). Hence, such sites promote ORR to proceed *via* a four-electron transfer mechanism. Recently, Kaukonen and co-workers calculated the oxygen adsorption energy on some transition-metal and nonmetal impurities doped graphene. Their results suggest that single P atom embedded in divacancies of graphene can be a good candidate for ORR due to the resultant low oxygen binding energy.¹⁰¹ These typical models involving the abovementioned active sites are provided in Fig. 1. One can see that the models used in theoretical studies are undergoing the transition from single atom to multi-atoms and hetero-atoms.

From the studies discussed above a conclusion was drawn that the adsorption of O_2 on graphene surface can be affected by doping, including the concentration and location of doping elements. In addition, for the first step in Scheme 1, the configuration of O_2 adsorbed on doped graphene impacts the

following steps (whether four-electron reduction to water, or two-electron reduction to hydrogen peroxide). Till date no direct observation is reported on the configuration of O_2 adsorbed on doped graphene surface, and two plausible models are proposed: (i) end-on adsorption through a single bond (Pauling model); (ii) bridge model with two bonds at two sites (Yeager model).^{129,136} The two-site configuration is likely to produce water *via* four-electron transfer involving the dissociation of O_2 , whereas single adsorption sites would probably generate hydrogen peroxide. Kim *et al.* performed adsorption barrier calculations for both models on doped graphene. The results showed that doped-N near the edge had considerably lower barriers of oxygen adsorptions, particularly for the end-on model.⁹⁰ In addition, Gong *et al.* suggested that N-doping may change the mode of oxygen adsorption from the end-on to side-on for carbon nanotubes, which will benefit the dissociation of O_2 and lead to four-electron reduction.³⁶

After the adsorption of O_2 on doped graphene, a more important step is that the first electron transfers to the adsorbed molecular O_2 , which has been widely accepted as the rate determining step (rds).¹³⁷ Using the energy difference (ΔO 2p) between the Fermi level and the peak position of density of states (DOS) in the unoccupied O-2p orbital for the adsorbed oxygen molecule, Kim and Tominaga *et al.* evaluated the transferability of the first electron to oxygen.^{89,90} The analysis shows that the existence of nitrogen reduces the ΔO 2p and facilitates the transfer of the first electron to oxygen. It is noteworthy that Tominaga *et al.* did not specify the ORR pathway (4e or 2e transfer), but took NH (pyridinic nitrogen) species of modified graphene as active sites for the ORR, whereas N_0 structure (graphitic nitrogen) on the edge was suggested by Kim *et al.* as the most probable or more active site toward the ORR than other structures. Moreover, Kim *et al.* proposed four-electron transfer as the preferred reduction pathway, which is widely accepted for doped graphene. In the following step, *viz.* the activation of oxygen on doped graphene surface, Xia *et al.* studied electrocatalytic mechanism of nitrogen doped graphene in acidic environment by DFT.⁸⁸ The simulation results on the electron transformation process (activation process of O_2) suggest a four-electron pathway ORR on N-graphene, with pure graphene being catalytically inactive toward ORR. For each reaction step, if nitrogen is introduced to graphene, the system energy decreases accordingly. Yu *et al.* obtained a deeper understanding of ORR reaction pathway for N-graphene by taking the effects of solvent, surface adsorbates, and coverage into consideration.⁸⁷ The key finding was that nitrogen doped graphene has comparable barrier of O_2 reduction to that of Pt (such as the steps of hydrogenation of $O_{2(ads)}$ or $O_{(ads)}$ and the removal of $OH_{(ads)}$). Therefore, it was suggested that O_2 is mainly reduced *via* “4e⁻ reduction” pathway on N-doped graphene.

Similar results were obtained on other heteroatoms doped graphenes. Fan *et al.* performed DFT calculations on ORR processes of B-doped graphene, in which the B sites were identified as the active catalytic centers where the largest amount of electron charges were depleted due to the relatively weak electronegativity of B atom.¹⁰³ Based on the charge-density

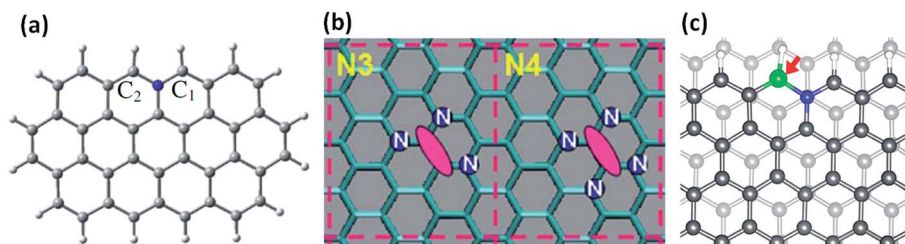


Fig. 1 (a) The cluster model of quaternary-N doped graphene catalyst. Grey is for carbon, white is for hydrogen, and blue is for nitrogen, reproduced with permission.⁹¹ Copyright 2013, Springer. (b) The model of N-doped graphene sheets. Adsorbed O₂ molecules are indicated by red ellipses, reproduced with permission.⁹² Copyright 2009, Elsevier, B.V. (c) Model structure of B/N doped graphene sheet at a zigzag-shaped step edge. Atom colors are grey for C, green for B, and blue for N, reproduced with permission.⁸⁶ Copyright 2010, American Chemical Society.

differences, the authors proposed the origin of catalytic activity as strong adsorption of OOH arising from the positive charge of active B sites and electron dipole. Moreover, in contrast to pure graphene the ORR processes for B-doped graphene were found to be exothermic by DFT calculations, which facilitates the charge-transfer thus a higher ORR catalytic activity.¹⁰⁰ As aforementioned, P-doped graphene can be a good candidate for ORR, whereas the active site is unclear. The electronegativity of P (2.19) is more negative than that of carbon, and charged sites (P⁺) on graphene can be created *via* P-doping that favor O₂ adsorption thus facilitating the ORR process. In experiment, P might exist in partially oxidized state thereby no longer act as the ORR active centers. To this, Li *et al.* claim the positively charged carbon atoms as actual active sites, which are created as the electrons were withdrawn to oxygen atom through the polarized bridge P atoms.⁷² The case is slightly different for S-doped graphene, as the S-doping is unlikely to significantly break the charge neutrality due to the close electron negativity of S and C. Consequently, the mechanism for S-doped graphene is also different from that of N-doped graphene. S-doping mainly induces more strain and defect sites in the graphene panel due to the larger atom radius and the change of spin density, which are attributed to the enhanced ORR activity of S-doped graphene. DFT calculations showed that reaction energy barriers of all ORR sub-reactions for S-doped graphene and platinum are comparable, indicating promising ORR activity of S-doped graphene.⁹⁸ More recently, a new concept of molecular doping of graphene was proposed. The ORR activity of the molecule-doped graphene can be enhanced by the charge-transfer process between the linked molecule (nitrobenzene) and graphene *via* a covalent bond.¹³⁸

Based on the discussions above, we can tentatively answer why the doped graphene shows higher catalytic activity but pure graphene is catalytically inactive toward ORR. The main viewpoints are summarized as follows:

(i) The difference in electronegativity of carbon and other heteroatoms induces polarization in the C–X bonds that facilitates the electron transfer. The electron-deficient atoms act as the adsorption and activation sites of O₂.

(ii) Heteroatoms doping results in the local high spin density, facilitating the adsorption of oxygen and formation of some intermediates.

(iii) Doped graphene possesses higher valence orbital energies of the ORR active atom to induce a smaller $\Delta O 2p$ (free energy difference), leading to lower kinetic stability and higher chemical reactivity.

3. The design and emerging approach of doped graphene

To date, various methods for the synthesis of heteroatom doped graphene and their ORR performance have been systematically reviewed and compared. Despite the significant cost reduction, the use of the currently available doped graphene is hindered by their unsatisfactory activity particularly in acid solution when compared with Pt-containing catalysts.¹³⁹ Fortunately, the abovementioned fundamental understandings on the origin of catalytic activity of doped graphene have been greatly improved in the recent few years and are now serving as a guide for the development of the next-generation ORR catalysts. One of the most promising approaches is to control the surface structure of doped graphene for higher ORR activity. Table 2 summarizes the major progresses in the synthesis methods, physical characteristics, and ORR activity of doped graphene. The basic designs include populating the number of active sites by increasing the content of doping element *via* new synthesis methods, controlling the doping forms (particularly for nitrogen doped graphene), developing co-doped graphene, and extending surface area of doped graphene, which are further elaborated below.

3.1. Populating the number of active sites

Generally speaking, doped graphene materials with higher content of dopants will provide larger population of active sites and thus higher catalytic activity toward ORR. Many attempts were made to increase the doped heteroatom content through various synthetic techniques, wherein the preparation methods were presented and discussed in details.^{119,121,124,126–128,144} As a whole, doped graphene has been realized mainly through two different ways: one is direct synthesis, such as chemical vapor deposition (CVD),^{64,77,145} solvothermal process,⁴⁸ segregation growth,¹⁴⁶ and bottom-up solution approach,^{147–149} and the other is post-treatment, including thermal treatment (*e.g.* thermally treating graphene

Table 2 Summary of heteroatom doped graphene (or graphene alloy) as electrocatalyst for ORR

Graphene alloy type	Synthesis method (precursors)	Heteroatom content, at% and doping forms	ORR performance	Electron transfer number	Ref.
N-graphene	Resin-based methodology (N-resin with $\text{CoCl}_2 \cdot 6\text{H}_2\text{O}$)	1.8 (pyridinic and graphitic-like)	60 mV lower in onset potential than Pt/C, with similar current density but higher stability	3.9 at -0.2 V	140
N-graphene	Thermal treatment (graphene and NH_3 800–1000 °C)	2.8 (pyridinic, pyrrolic, graphitic-like N)	Comparable activity with Pt/C, but higher durability	~4 at -0.5 V	50
N-graphene	Plasma (N_2)	8.5 (pyridinic, pyrrolic, graphitic-like N and N-oxides)	Higher activity than graphene, and higher durability and selectivity than Pt/C	Not mentioned	141
N-graphene	Detonation technique (cyanuric chloride and trinitrophenol)	12.5 (pyridinic, pyrrolic, graphitic-like N)	The same CV curves, better stability than Pt/C	3.69 at -0.4 V	49
N-graphene	CVD ($\text{NH}_3/\text{He}:\text{C}_2\text{H}_4:\text{H}_2$)	0–16 (pure pyridinic N)	-0.3 V onset potential, poor activity compared to Pt disk	2 from -0.4 to 0.6 V	142
N-graphene	Solvothermal (Li_3N , CCl_4 with or without $\text{N}_3\text{C}_3\text{Cl}_3$)	4.5–16.4 (pyridinic, pyrrolic, graphitic-like N)	Comparable current density with Pt/C, negative onset potential compared with Pt	Not mentioned	48
N-graphene	Direct synthesis (glucose and urea)	24–25 (pyridinic and graphitic N)	Comparable ORR activity with Pt/C, but higher fuel crossover resistance and stability	3.7 at -0.9 V	143
B-graphene	Solvothermal method (CCl_4 , BBr_3 , K)	1.02–2.56 (B–C, higher binding energy for B 1s)	Not mentioned	Not mentioned	52
B-graphene	Thermal treatment (graphene oxide and B_2O_3)	3.2 (B–3C and edge B–2C–O)	Higher activity than graphene, and long-term stability	3.5 from -0.4 to -0.9 V	108
B-graphene	Thermal treatment (graphene oxide, H_3BO_3 900 °C)	3.6 (B–C and B–C–O)	Comparable activity with N-graphene, higher stability than Pt/C	3.09	80
S-graphene	CVD (thiophene with Fe–Co/ γ - Al_2O_3 as catalyst)	3.2 (–C–S–C– and –C– SO_x –C–)	Similar activity to N-graphene	3.4 at -0.25 V	77
S-graphene	Thermal treatment (graphene oxide and benzyl disulfide, 600–1050 °C)	1.30–1.53 (–C–S–C– and –C– SO_x –C–)	Higher activity and selectivity than Pt/C	3.82 at -0.3 V	54
P-graphene	Thermal treatment (graphite oxide and triphenylphosphine, 1000 °C)	1.81 (P–C and P–O bonds)	Higher activity than graphene, and higher selectivity than Pt/C	3.0 to 3.8	43
B,N-graphene	CVD (melamine, boric acid on nickel foam)	N: 4.5, B: 3 (B–C, B–N, B–O)	Onset potential (-0.16 V vs. -0.01 V of Pt/C), higher current density than Pt/C	3.4–3.8 from -0.2 to -0.5 V	107
B,N-graphene	Thermal treatment (graphene oxide, NH_3 , H_3BO_3 900 °C)	B: 2.17, N: 4.42 (B–C and B–C–O) (pyridinic, pyrrolic, graphitic-like N)	Close onset potential and current density to Pt/C, higher stability than Pt/C	3.81	80
S,N-graphene	Thermal treatment (graphene oxide, melamine and benzyl disulfide, 900 °C)	N: 4.5, S: 2.0 (–C–S–C–) (pyridinic, pyrrolic, graphitic-like N)	Higher activity than S-graphene and N-graphene, comparable ORR performance to Pt/C	3.6 at -0.6 V	57
S,N-graphene	Hydrothermal process (ammonium thiocyanate and graphene oxide)	N: 12.3 (pyridinic and graphitic N), S: 18.4 (C– S_n –C and –C=S–)	Comparable ORR current density to Pt/C	3.9 from -0.1 to -0.7 V	75
P,N-graphene	Pyrolysis (graphene–dicyandiamide–phosphoric acid)	P: 0.4, N: 5.1 (P–C, P–O, and P– Me_x) (pyridinic, pyrrolic, graphitic-like N)	1.8 times higher mass current density than N-graphene (in 0.1 M HClO_4)	3.96 at 0.75 V	70

oxide with nitrogen-containing compounds at high temperature), arc-discharge, and plasma treatment.^{44,47,50} For B, S, or P doped graphene, only limited methods (such as CVD or thermal treatment method) have been reported. Recently, solvothermal process under lower temperature was proven to be feasible to prepare B or S doped graphene.^{52,68} In B, S, and P doped graphene, the doping content achievable till date was

at most 4.3%, 3.2%, and 1.8%, respectively.^{64,72,77} More approaches need to be developed to further increase the doping content.

In contrast, more techniques are available to obtain nitrogen doped graphene with nitrogen doping at a wide range of doping content in varied doping forms, populating the number of the active sites to a desirable range. CVD technique produces N-

graphene at large area in high-quality with the nitrogen content tunable from 0% to 16% by changing the N-containing precursors.¹⁴² However, the dependence of CVD method on a Cu or Ni foil surface for N-graphene film growth and the tedious and costly post-removal of Cu or Ni substrate makes it economically less practical. Physical treatment (arc-discharge and plasma) is suitable for the large scale preparation of high quality N-graphene.^{46,140,150} Arc-discharge method generally delivers a doped nitrogen content of as low as 1%;⁴⁶ whereas plasma treatment is able to produce tunable content of doped nitrogen by varying the plasma intensity and exposure time¹⁵⁰ with a demonstrated maximum content of 8.5%.¹⁴⁰ Thermal treatment, however, has been the most widely used approach to introduce nitrogen into graphene frameworks due to its simplicity. Many nitrogen-rich compounds, such as ammonia, urea, hydrazine, melamine, polyaniline, cyanamide, pyrrole, and 5-aminotetrazole monohydrate, have been employed as the sources of nitrogen atoms.^{50,53,58,59,61,63,66,71,73,76,78,79,151–155} In these attempts, the nitrogen doping content achieved were mostly about 2–5%, except the high temperature treatment of graphene oxides with melamine or 5-aminotetrazole monohydrate conducted by Lu and Sheng *et al.* that delivers a high content nitrogen doping of about 10%.^{53,73}

Different from the energy-intensive high temperature (800–1100 °C) thermal treatment approach, solvothermal process that works at a considerably lower temperature comes out as a more favorable alternative, which delivers products in large quantity through easy-to-operate procedures. In particular, the content of nitrogen doping in this case can be as high as 16.4%, if lithium nitride (Li₃N) is mixed with tetrachloromethane (CCl₄) or cyanuric chloride (N₃C₃Cl₃) with Li₃N and CCl₄ and treated at ~300 °C in an autoclave.⁴⁸ Further increase of

nitrogen doping content was realized by Zhang *et al.* in a two-step method, in which N-doped graphene was synthesized using reactive graphitic carbon and N-rich molecules (*e.g.* melamine and urea) as starting materials.¹⁴³ The doped nitrogen content achieved in this case was generally 24–25%, and the 33% of nitrogen doping therein tops the record till date (Fig. 2). The ORR on such N-graphene exhibits favorable water formation *via* a four-electron pathway, and the performance is comparable to commercial Pt/C. Moreover, such N-graphene shows considerably better fuel crossover resistance and long-term stability in alkaline medium, promising great potential in practical applications. It is noteworthy that the correlation of high population of active sites with high N-content may not uniformly work for all forms of doped-nitrogen. In the co-existence of nitrogen in different doping forms, the situation gets more complicated. To answer if the ORR activity mainly arises from one form of doped nitrogen, or a fairly equally important co-contribution *via* a synergistic effect of two or more forms of doped-nitrogen, it is essential to synthesize doped graphene with high purity of a single form of N-doping and get them thoroughly investigated with the assistance of advanced characterization techniques. The control of nitrogen doping and the effect are discussed in details in the following section below.

3.2. Controlling the doping forms

The heteroatoms may adopt different configurations in doped graphene, forming C–X (possible also X–O) as the active sites for ORR. The configuration for B, S, or P elements doped graphene is relatively simple, whereas four kinds of nitrogen forms (graphitic N, pyridinic N, pyrrolic N, and pyridinium N) may present concurrently in N-doped graphene due to the

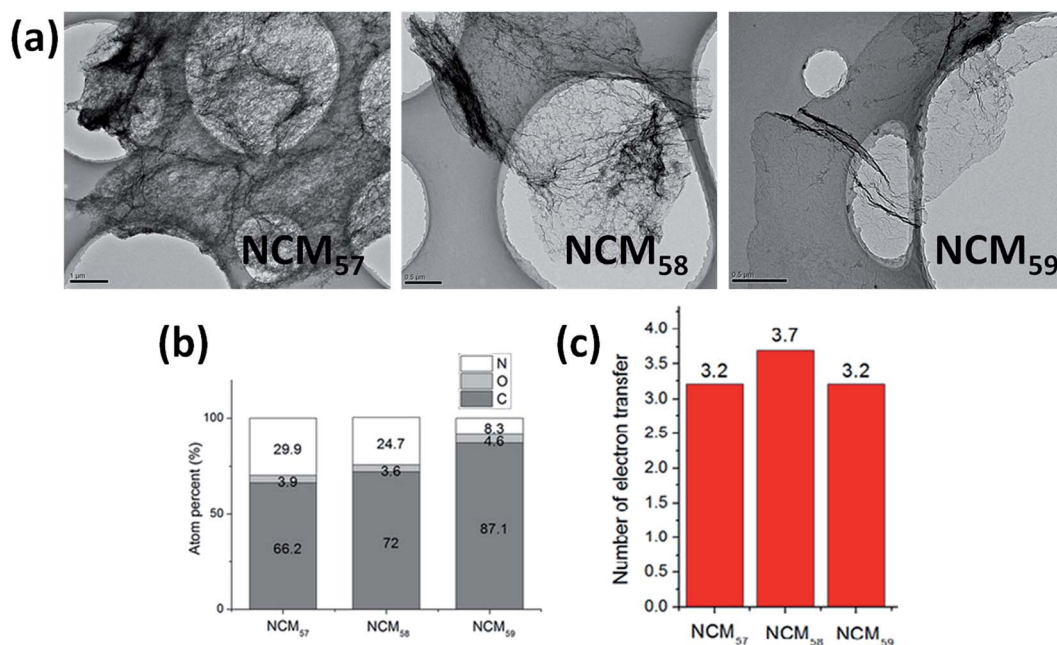


Fig. 2 (a) Typical TEM images of N-doped graphene. (b) The content of C, N, and O in three samples by XPS. (c) Electron-transfer numbers at –0.9 V; reprinted with permission.¹⁴³ Copyright 2013, Macmillan Publishers Ltd.

comparable atomic size of N and C and the strong covalent bonds between them. Theoretical calculations are unable to provide any straightforward answer which form of nitrogen is the actual active center. On the experimental side, Sun *et al.* claimed that quaternary type (graphitic) nitrogen species contribute the most to the ORR activity,⁵⁰ which was supported by the results of Lin *et al.* in a separate study.¹⁰⁶ In contrast, the experiments of Woo and Xia *et al.* suggested the pyridine like N as the determining structure for the electrocatalytic activity of N-doped graphene toward ORR.^{53,152} A further view held by Dai *et al.* on N-doped graphene is that higher catalytic activity originates from the presence of pyridinic and pyrrolic N species.^{32,36} More specifically, Ruoff *et al.* suggested that increasing pyridinic N species content might lower the onset potential of oxygen reduction and gradually switch the ORR reaction mechanism from 2e dominated process to 4e dominated process, whereas graphitic-N content was related to the limiting current density.¹⁵⁴ Despite these findings, it is difficult to specify the role of each type of nitrogen species in the ORR activity of N-graphene. To address this issue, it is desirable to have doped graphene with single N-species synthesized. Wong *et al.* synthesized N-graphene with a high content of graphitic N (purity: 44%) by pyrolyzing a mixture of graphene oxide and polypyrrole, in which the pyrolysis temperature and the selection of N-precursor were found to be critical to the ratio of different N-species in the doped graphene.¹⁰⁶ Ruoff *et al.* investigated the thermal reaction of GO with various N-precursors using annealing method.¹⁵⁴ It showed that with ammonia the doped graphene preferentially have graphitic N and pyridinic N centers, whereas polyaniline and polypyrrole tend to produce pyridinic and pyrrolic N moieties in the doped

graphene, respectively. Sun *et al.* used an uncommon organic compound, pentachloropyridine, as C and N precursor to synthesize N-doped graphene *via* solvothermal method.⁵⁵ The unique structure of the precursor led to the formation of only two types of nitrogen, *i.e.* pyridine-like (60.1%) and graphitic-like (39.9%) nitrogen. Nitrogen doped graphene with high purity of either pyridinic or quaternary nitrogen species were selectively synthesized recently *via* temperature-induced surface polymerization reaction using pyridine and julolidine as monomers, respectively.¹⁵⁶ Pyridine-based N-graphene comprised high purity of pyridinic N (90%) whereas julolidine-based N-graphene primarily contained quaternary N with a purity of 80%. Apparently, in multiple-N species containing N-graphene produced *via* thermal method it is possible to have one type of N as the dominant component. More recently, Sinitskii *et al.* demonstrated an approach based on Yamamoto coupling of N-doped molecular precursors and cyclo-dehydrogenation that produced high-quality graphene nanoribbons (Fig. 3).¹⁴⁹ The X-ray photoelectron spectroscopy (XPS) N 1s spectrum presented a single peak at 391.1 eV, which was close to pyridinic nitrogen peak in N-graphene. These bottom-up methods opened a new door to the preparation of single N-doped graphene.

3.3. Developing co-doped graphene

Heteroatom (N, B, S, P, *etc.*) elements were introduced into graphene to tailor the electron-donor properties of this 2D material and consequently to enhance its catalytic activity. Despite their improved ORR catalytic activity compared to the pristine graphene, the mono-heteroatom doped graphene

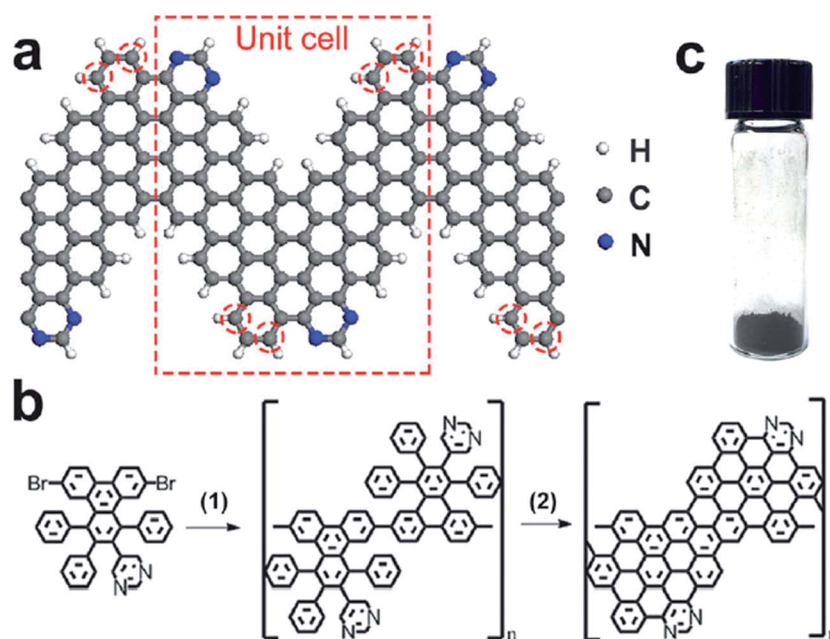


Fig. 3 Synthesis of 4N-graphene nanoribbons (4N-GNRs). (a) Schematic of 4N-GNR. (b) Reaction scheme used in this work: (1) Yamamoto coupling, (2) Scholl reaction. (c) Optical photograph of a 4N-GNR powder. Reproduced with permission.¹⁴⁹ Copyright 2014, The Royal Society of Chemistry.

materials only manifested moderate ORR performance in alkaline solution. The co-doping of graphene with two or more different heteroatoms that enables complex electrical and physical modifications of graphene was taken as a new strategy to further improve the ORR activity. Among the known dopants, nitrogen and boron are seen as the best co-dopants due to their comparable atomic size and the presence of five or three valence electrons available to form strong bonds with carbon atoms, respectively.⁶⁴ An earlier computational study by Ikeda *et al.* revealed that those particular N-dopant configurations with the ability of the catalytic activity enhancement were less stable than those configurations that potentially suppress the catalytic activity.⁹³ Fortunately, this dilemma has been partially reconciled *via* the co-doping of boron and nitrogen. On one hand, the strong attractive interaction between neighboring B and N enables N dopants to occupy a particular site suitable for the catalytic activity enhancement. On the other hand, the B–N co-doping is able to activate the catalytically inert sites in the corresponding single-dopant configurations. Therefore, free-energy barriers are remarkably reduced for O₂ adsorption and the subsequent reduction process, allowing for the enhancement of the ORR activity with stable dopant structures.⁸⁶ For instance, BCN graphene prepared by Dai *et al.* *via* thermally annealing GO in the presence of boric acid and ammonia has proven to be superior to the commercial Pt/C in electrocatalytic activities (Fig. 4a). The first-principle calculations revealed that compared to the pure graphene, BCN graphene possesses high population of carbon atoms with relatively high spin density and charge density, which are two key factors determining the catalytic capability of a material toward ORR as discussed in the second section of this work. In addition, BCN graphene with a moderate level of N- and B- doping has lower energy gap, indicating higher chemical reactivity.⁶² B, N-graphene synthesized by Qiao *et al.* *via* a two-step doping method⁸⁰ also showed greatly improved ORR activity with high selectivity of four-electron ORR pathway in an alkaline medium, which is considerably higher than that observed for single B- or N- doped graphene (Fig. 4b). A new B–C–N configuration was identified as the active site, with enhanced synergistic effect from the chemical coupling of B and N accounting for the boost of the ORR activity. Such synergistic effect was also seen in N, S co-doped graphene. As N and S are concurrently incorporated into graphene, the dual activation of carbon atoms increases the charge/spin densities, resulting in greatly improved catalytic activity in terms of more positive onset potential and higher kinetic limiting current on N, S-graphene as compared to that of N-graphene or S-graphene (Fig. 4c).⁵⁷ Apart from B/N and S/N co-doped graphenes, P/N co-doped graphene synthesized by Woo *et al.* is another example that shows onset potential of 0.87 V with mass activity of 0.80 mA mg⁻¹, which was 1.8 times higher than that of the N-doped graphene (Fig. 4d).⁷⁰ Similarly, the improved ORR activity was believed to originate from the electrophysical modification of N-graphene by the introduction of the additional dopant of P, which enhanced the asymmetry of spin density and facilitated electron transfer on the graphene basal plane. One would be interested if an order of catalytic activity was available based on the different doping elements, such as B, N, P, and S. To this,

Qiao *et al.* provided a useful ORR free energy diagram for model catalysts (B, N, P, S, O doped graphenes) by obtaining the free energy for each reaction step of “4e-reaction pathway”.¹⁵⁷ In the diagram, nitrogen- and boron-doped graphene models exhibit the lowest overall reaction free energy change, suggesting the best ORR performance from the theoretical viewpoint. An order of catalytic activity in the sequence of B-graphene > N-graphene > P-graphene > S-graphene seems conclusive in this case. Nevertheless, it has to be noted that practically more factors could alter this order, *e.g.* dopant content, doping types and morphological properties, which may not be achievable in the same way and at the same level for different dopants. Apparently, by taking advantages of different heteroatoms in conjugated graphene backbone that creates new charged sites favorable for O₂ reduction, the co-doping of graphene, in particular the additional doping to N-graphene, is becoming one of the main trends in further improving ORR activity of such 2D materials.

3.4. Extending surface area of doped graphene

Undoubtedly, heteroatom doping that creates more active sites of ORR in doped graphene has played a significant role in boosting the ORR catalytic activity. The efforts in increasing the total number of active sites by increasing the heteroatoms content or co-doping have been reviewed above. It is understood that active sites must be accessible, *e.g.* exposed to the surface, in order to contribute to the ORR activity. However, just like graphene sheets, doped graphene sheets also tend to form irreversible agglomerates or even restack back to graphite-like structure due to strong π – π stacking and the inter-sheets van der Waals interactions, resulting in a significant decrease in the surface area. As a result, a large population of “active sites” are walled inside the catalyst and become inaccessible for ions and gases, and the inefficient ionic and electronic transport lead to unsatisfactory electrocatalytic capabilities. To maximize the utilization of the active sites, the accessible electroactive area is enlarged or extended by changing the morphology and “particle” size of doped graphene, such as three dimensional (3D) structures,¹⁵⁸ porous structures^{153,159–163} and doped graphene quantum dots.^{164,165} As graphene-based materials exhibit strong direction dependent thermal and electrical transport properties with extremely low out-of-plane conductivities, 3D network or porous structures will provide not only high specific surface area, but also the possibility of extending the unique properties of doped graphene into three dimensions.^{63,65,66,68,71,75,104,107,166} Recently, Dai *et al.* reported 3D graphene foams doped with nitrogen, boron or both, prepared by CVD method.¹⁰⁷ Electrochemical studies show high electrocatalytic activities toward ORR for B/N co-doped graphene foams, which outperforms Pt/C in terms of peak current of oxygen reduction. Differently from what was discussed in the previous sections, the high catalytic activity in this work was also attributed to the significantly increased electrochemically active surface areas from the 3D network structure, apart from the synergetic effect of B and N co-doping. Another example demonstrated by Feng *et al.* is nitrogen and sulfur co-doped 3D graphene frameworks, synthesized *via* a one-pot low

temperature approach.⁷⁵ Using thiocyanate as N/S dual-containing precursors, the as-prepared N/S-co-doped graphene exhibits a surface area of $220 \text{ m}^2 \text{ g}^{-1}$ and high ORR catalytic activity of 4e transfer dominated pathway with kinetic limiting current density comparable to Pt/C but an even higher selectivity. The significance of the 3D structure was further demonstrated by Shi *et al.* through evaluation of the oxygen reduction performance of doped graphenes of different morphology with single dopant, *e.g.* S-doped graphene sheet and S-doped graphene 3D foam.⁶⁸ Although the sulfur content in S-doped graphene sheet is considerably higher than that in S-doped foam, the oxygen reduction performance of the former is found inferior to that of the latter. Unfortunately, few reports on 3D porous doped graphene in contrast to the 3D porous graphene are available. Anyone interested can refer to some recent reviews on the detailed process of the preparation and characterization of porous graphene.^{158,160} In principle, the methods for the

preparation of porous graphene can be adopted to synthesize 3D porous doped graphene.^{167–169} For 3D porous graphene, a representative method developed by Bando's group was a sugar-blowing technique, in which a 3D self-supported graphene bubble network (strutted graphene or shortened as SG, *cf.* Fig. 5) with a specific surface area of $1005 \text{ m}^2 \text{ g}^{-1}$ can be harvested.¹⁶⁸ Naturally, synthetic protocol can be envisaged as a general path for the synthesis of 3D doped graphene with some modifications (perhaps by post-treatment or by changing the precursors). Such 3D porous structures with high surface area not only expose more active sites, but also facilitate fast mass and electron transport kinetics during the ORR process. Therefore, it can be foreseen that more novel 3D porous structures of doped graphene with enhanced ORR activity will be springing up soon.

Apart from creating 3D or porous structures, surface area can also be increased by reducing the “particle” size of graphene-based materials. Bao *et al.* prepared graphene in nanometer size

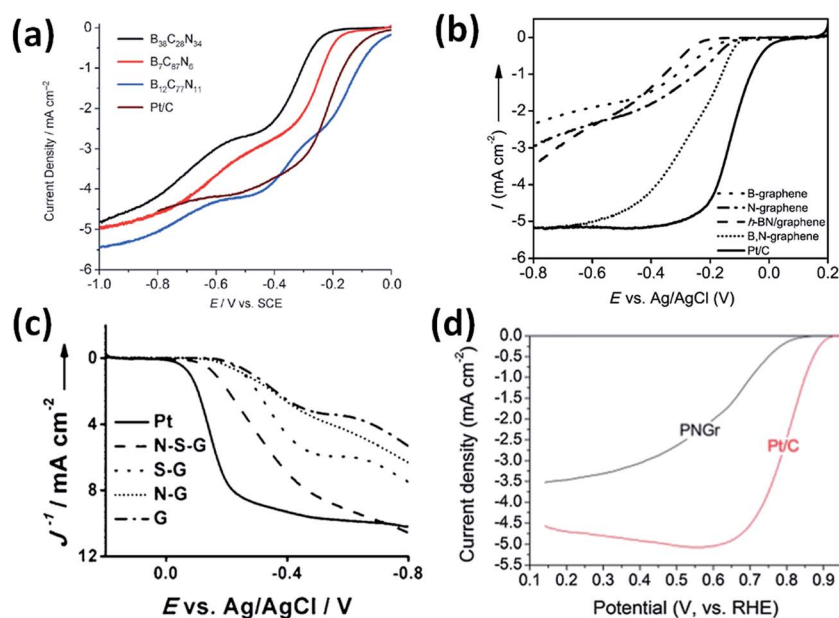


Fig. 4 ORR performance on various co-doped graphene materials as compared to commercial Pt/C. (a) Linear sweep voltammetry (LSV) curves of ORR on BCN graphene with different compositions in oxygen-saturated 0.1 M KOH solution at 10 mV s^{-1} , reproduced with permission.⁶² Copyright 2012, Wiley-VCH. (b) LSV of various electrocatalysts on a rotating disk electrode (1500 rpm) in an O_2 -saturated 0.1 M KOH (scan rate: 10 mV s^{-1}), reproduced with permission.⁸⁰ Copyright 2013, Wiley-VCH. (c) LSV of different samples at 1600 rpm in an O_2 -saturated 0.1 M KOH, reproduced with permission.⁵⁷ Copyright 2012, Wiley-VCH. (d) ORR result of P/N doped graphene as compared to that of Pt/C in 0.1 M HClO_4 with a 900 rpm rotation speed, reproduced with permission.⁷⁰ Copyright 2013, The Royal Society of Chemistry.

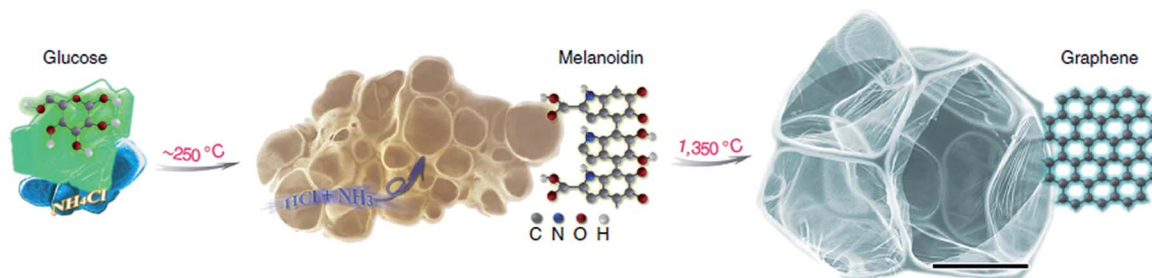


Fig. 5 Growth process and structural regulation of sugar-blowing production, reprinted with permission.¹⁶⁸ Copyright 2013, Macmillan Publishers Ltd.

scale *via* direct ball milling of graphite-based materials, and the size effect of crystals of graphite nanosheets in electrocatalytic activation of oxygen was clearly observed.¹⁷⁰ More recently, Wang *et al.* provided direct evidence from electrochemical studies using a designed micro apparatus to support the argument that the edge of a graphite is more active than the basal

plane toward ORR.¹⁷¹ With smaller size, graphene nanosheets become more active in the oxygen reduction reaction, which may be ascribed to the increasing number of edge sites (*e.g.* zigzag edges). Theoretical calculation showed that the catalytic activity of doped graphene (N-graphene) is closely linked to the location of incorporated N in the graphene matrix,

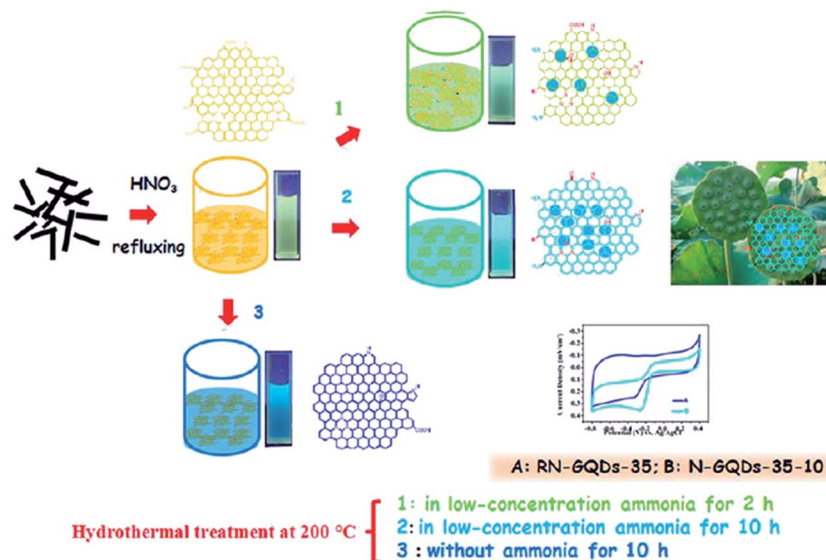


Fig. 6 Strategy for the synthesis of nitrogen doped graphene quantum dots hybrids, reproduced with permission.¹⁷⁴ Copyright 2013, American Chemical Society.

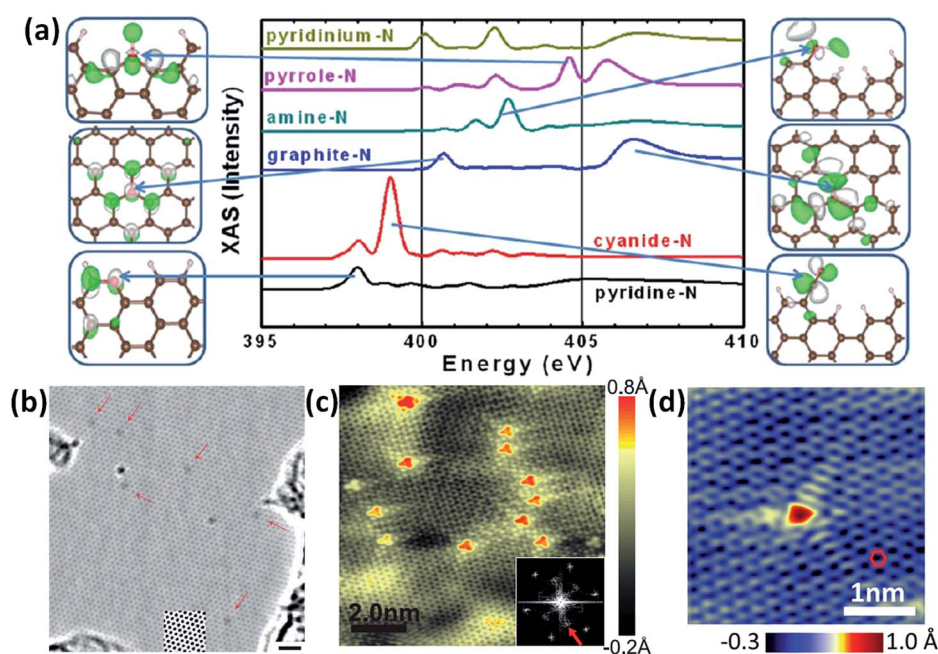


Fig. 7 The advanced characterization techniques for identifying the dopants atoms. (a) Calculated K-edge X-ray adsorption (XAS) spectra of N in the various configurations, reproduced with permission.¹⁷⁶ Copyright 2013, American Chemical Society. (b) HR-TEM image of N-doped graphene showing six nitrogen substitution defects marked by red arrows, reprinted with permission.¹⁷⁹ Copyright 2011, Macmillan Publishers Ltd. (c) STM image of N-doped graphene on copper foil showing 14 graphitic dopants and strong inter-valley scattering tails, reprinted with permission.¹⁸⁰ Copyright 2011, American Association for the Advancement of Science (AAAS). (d) STM imaging of a single graphitic boron dopant, the most common doping form observed on B-doped graphene on copper foil, reproduced with permission.¹⁸² Copyright 2013, American Chemical Society.

in which the doped N atoms near the edge of graphene sheets are more desirable active sites for improved electrocatalytic activity. This has been proven experimentally by Zhang *et al.* recently in edge-nitrogen-rich graphene nanoplatelets prepared *via* a combined process of ball milling of graphite powder with melamine and subsequent heat treatment.¹⁷² Through the process the pristine graphite flakes with a size of $\sim 270 \mu\text{m}$ (50 mesh) was converted to nanoplatelets in the size of $\sim 500 \text{ nm}$, and the surface area was greatly increased. The high ORR activity was a result of synergetic effects of edge-N-doping and the extended surface area arising from the formation of nanostructured platelets. In addition, if a process is able to minimize defects introduction into graphitic matrix and keep graphene inner basal plane intact, it will help retain the electrical conductivity and facilitate charge transport during electrocatalysis. To this, Li *et al.* synthesized N-doped colloidal graphene quantum dots (QDs) with well-defined structures and varied sizes *via* a solution chemistry approach, and the product was found to catalyze ORR *via* a four-electron reduction pathway.¹⁶⁵ Interestingly, their studies showed higher activity for the larger N-doped QDs (176 carbon atoms) rather than for that of 128 carbon atoms.¹⁷³ Similarly, higher catalytic activity of N-doped QDs toward ORR was shown by Wu *et al.* in a novel lotus seedpod surface-like pattern of 0D seed-like N-doped QDs (3 nm) docked on the surface of 2D N-doped QDs sheets of $\sim 35 \text{ nm}$ (Fig. 6) prepared by ammonia-mediated bond-scission strategy.¹⁷⁴ Such N-doped QDs structure presents a four-electron catalysis process toward ORR with higher selectivity and durability compared to commercial Pt/C electrode. Unfortunately, the information on the surface area of these N-doped graphene QDs were not reported, although a detailed characterization of surface area will facilitate the understanding on the size effect of such materials with respect to their ORR activity. Such graphene quantum dots, the graphene sheets with lateral dimensions less than 100 nm in single, double, and few layers (3 to <10 layers), are rising stars in graphene family and will continue to attract attention in the fields of materials science and engineering.⁸² With nanosheets as supporting substrates, nitrogen doped QDs are anticipated to give unique properties in further improvement of ORR catalytic activities due to the possible synergy of vast surface area, quantum confinement, and edge effects.

4. Conclusions and perspective

In this review, we focused on the doped graphene as efficient non-metal catalysts toward ORR. Firstly, the mechanism of oxygen reduction by doped graphene is extensively reviewed. The theoretical calculations showed that single, dual, or even multi-doping of heteroatoms may break the distribution balance of the electron spin density or atomic charge density on the plane of graphene, thus changing their electrocatalytic activity. Generally, atoms with higher spin density or more positive charges are probably the catalytic active centers. Does bigger difference in the electronegativity of atom carbon and heteroatom mean higher ORR activity? This is a natural question to be asked. Unfortunately, lack of convincing evidences on

the ORR catalytic activity comparison among different heteroatom doped graphenes excludes any specific correlation between inter-element electronegativity difference within doped graphene and its ORR activity. The presence of an electronegativity difference is not even a prerequisite for doped graphene to be ORR active. A typical example is ORR active S-doped graphene, in which sulfur has the electronegativity very close to that of carbon and electron transfer hardly takes place. To explain this phenomenon, some researchers proposed that the spin density is probably more important than atomic charge density in determining the catalytic active sites. Although it is proven that heteroatoms doping makes graphene more catalytically active toward ORR, more intensive efforts are needed to provide evidences or theoretical supports on how ORR activity was improved in these different heteroatoms doped graphenes. In experiments, doped graphenes have shown the capability of catalyzing oxygen reduction *via* 4e transfer pathway; and importantly, some of them even outperform commercial Pt/C in terms of durability and selectivity apart from the considerably lower materials cost, promising great potential in replacing conventional Pt/C catalysts in applications using alkaline electrolyte. Nevertheless, for applications requiring acidic electrolyte, these doped graphenes are still unable to compete with commercial Pt/C catalysts. This remains a challenge for future research.

A good understanding on the origin of ORR activity enhancement in heteroatom-doped graphene is the prerequisite for further improving these non-noble metal catalysts. To date, the detailed ORR mechanism involving the real active centers is incomplete, and the nature of intermediates in the reduction process remains vague. The theoretical study is constrained by simple models and small-sized systems, which is difficult to provide quantitative numbers for detailed reaction steps. A powerful model and more theoretical studies will help to provide deeper understanding on ORR of doped graphene, and in turn facilitate design of new electrocatalysts with further improved ORR activity. In experiment, the emerging solution chemistry approaches that produce graphene quantum dots with nitrogen and other atoms in various bonding configurations provide unique opportunities for systematic investigation on the mechanism of the ORR catalysis and identifying the real active sites for nitrogen doped graphene materials. In particular, the doped graphene quantum dots with sizes closer to those used in the models of theoretical studies are especially useful, as it provides the closest possible matching for the theoretical and experimental results.

The general understanding is that the heteroatom content of doped graphene is closely related to the electrochemical ORR activity. Low heteroatom content provides too few active sites to boost the catalytic activity toward ORR, whereas high heteroatom content may result in low conductivity whereby more active sites are prone to poisoning. Therefore, appropriate heteroatom content in graphene that keeps high population of active sites while maintains reasonable conductivity is desirable. This requires further work to exploit new methods to manage heteroatom doping with optimal doping content. In addition, electrochemical activity is strongly influenced by the

types of heteroatoms. As presented above, there are at least four types of nitrogen (pyridinic, pyrrole, graphitic N, and N-oxides) in N-doped graphene, and different bond configurations such as B–C, B–O, S–O, S–C, and P–C, P–O in B, S, and P doped graphene, respectively. The situation is more complicated for dual- or even multi-heteroatoms doped graphene. In such cases, it is unclear if S, P and other bigger sized heteroatoms substitute carbon atoms in the sp^2 network of graphene like what N or B atom does. For N-doped graphene, how the different N affects the ORR activity remains controversial. As for co-doped graphene, both the location and ratio of heteroatoms, such as B/N, S/N, and P/N, impact the ORR activity. The exact mechanism has not been investigated in detail yet due to the lack of experimental data. Apart from developing synthetic techniques with good control for the specific type of heteroatoms, the in-depth knowledge about the active sites relies on the accuracy of characterization data obtained from these doped graphene structure. XPS technique is the commonly used technique to identify most of heteroatoms configurations;^{41,175–177} however, the assignment of some spectral features is often debatable. For example, Ray *et al.* assigned the N 1s XPS peak at around 399.9–400.2 eV to cyanide-like N,¹⁷⁷ whereas Pels *et al.* ascribed the same peak to pyrrole-like N.¹⁷⁸ In addition, it is difficult to distinguish pyridinic N from graphitic N at the edge experimentally, as they are essentially same in structure. For S-doped graphene, despite the same synthesis method used, the S 2p peak was assigned only to –C–S–C– structure by some groups,^{57,81} whereas others take it as a mixture configurations of –C–S–C– and –C–SO₂–C–.^{54,65,69} To ensure less controversial assignment, Wang *et al.* suggested combining XPS, X-ray adsorption spectroscopy (XAS), and X-ray emission spectroscopy (XES) with theoretical analysis to identify most of the N configurations in graphene-based materials (Fig. 7a).¹⁷⁶ XAS is able to determine the N structures in the π states more accurately, and provide direct information on the correlation of the types of N with the ORR activity. In addition, by combining high-resolution transmission electron microscopy (HR-TEM) images with first-principle electronic structure calculations, Meyer *et al.* investigated the electronic configurations of nitrogen substitution point defects in graphene sheets.¹⁷⁹ In this case, the doped nitrogen exhibits a weak dark contrast in the large defocus HR-TEM images (Fig. 7b), providing experimental evidence for strong chemical bonding induced charge transfer from the carbon atoms to the region of the bond with the neighbouring nitrogen atom. Using scanning tunneling microscopy (STM), Zhao *et al.* clearly visualized individual nitrogen dopants in monolayer graphene.¹⁸⁰ The STM observations indicate that the majority of the doping occurs *via* graphitic substitution in the sample (Fig. 7c). We believe that in near future the systematical analysis by combining high resolution electron microscopy^{181–184} and synchrotron spectroscopy characterization techniques with theoretical structure calculation will be able to further decode the mystery, revealing the structure and configurations of the dopants in detail more accurately.

It is also worth noting that the existence of trace metal (below the detection level of XPS) as MeN_x active site,²⁵ or Me–C coordination,⁴² or metal oxide on doped graphene¹⁸⁵ might have

profound influences on the ORR. Therefore, doped graphene from treatment of graphene oxide, derived from commercial graphite containing impurities in the order of parts per million (ppm) *via* Hummers method whereby permanganate is introduced, will probably suffer from a contamination of some metal impurities. In this case, elemental analysis of metal contents in doped graphene is essential to support the claim of ORR activity originates from the heteroatoms induced active sites in the carbon lattices. Moreover, the most frequently used technique for ORR catalysis studies is the linear sweeping voltammetry based on rotating disk electrode (RDE) and rotating ring-disk electrode (RRDE).^{186,187} The calculations for the number of electron transferred based on Koutecky–Levich plots from RDE were derived for smooth electrode surface. However, for the doped graphene catalysts, a thick catalyst film (>25 μm) with uneven surfaces is typically used. Technically speaking, Koutecky–Levich equation is not applicable in this case with rough surfaces. Moreover, for RRDE, the peroxide formed is completely quenched within the catalyst layer and hence is not detected at the ring electrode. The elimination of peroxide in this case may cause difficulties in the identification of the ORR pathway. Therefore, a standard protocol needs to be established and calibrated to evaluate the ORR activity on doped graphene materials. Furthermore, there is no way to measure area density of active sites for Pt/C catalysts, and thus, the gravimetric current density should be used as the criterion for the performance comparison. Moreover, in most of experimental approaches, the graphene alloy catalysts for ORR were evaluated in half-cell reaction. To enable the practical applications of doped graphene as electrocatalysts, full-cell test experiment would be more appropriate and should be seriously considered in future.

We firmly believe that the combination of heteroatoms doping and special features introduction is a promising approach for the development of “graphene alloy” with high electrocatalytic activity. Unquestionably, the main focus for the next few decades will be the further development of novel doped graphene materials and the understanding of active sites through experimental approaches and theoretical investigations with the help of advanced characterization techniques. In this sense, it is anticipated that such development will accelerate the implementation of any newly doped graphene catalysts approaches into actual electrodes.

Acknowledgements

This work is supported by the project of IMRE/12-2P0504, which is part of the Advanced Energy Storage Research Programme, funded by the Science and Engineering Research Council (SERC) of A*STAR (Agency for Science, Technology and Research), Singapore.

Notes and references

- 1 J.-H. Wee, *Renewable Sustainable Energy Rev.*, 2007, **11**, 1720–1738.

- 2 G. Farmer and D. J. Hamblin, *First on the Moon*, Little, Brown and Company, 1970.
- 3 A. Rabis, P. Rodriguez and T. J. Schmidt, *ACS Catal.*, 2012, **2**, 864–890.
- 4 M. K. Debe, *Nature*, 2012, **486**, 43–51.
- 5 Z. Chen, D. Higgins, A. Yu, L. Zhang and J. Zhang, *Energy Environ. Sci.*, 2011, **4**, 3167–3192.
- 6 B. Wang, *J. Power Sources*, 2005, **152**, 1–15.
- 7 H. A. Gasteiger, S. S. Kocha, B. Sompalli and F. T. Wagner, *Appl. Catal., B*, 2005, **56**, 9–35.
- 8 V. R. Stamenkovic, B. Fowler, B. S. Mun, G. Wang, P. N. Ross, C. A. Lucas and N. M. Markovic, *Science*, 2007, **315**, 493–497.
- 9 V. R. Stamenkovic, B. S. Mun, M. Arenz, K. J. J. Mayrhofer, C. A. Lucas, G. Wang, P. N. Ross and N. M. Markovic, *Nat. Mater.*, 2007, **6**, 241–247.
- 10 J. Greeley, I. E. L. Stephens, A. S. Bondarenko, T. P. Johansson, H. A. Hansen, T. F. Jaramillo, J. Rossmeisl, I. Chorkendorff and J. K. Nørskov, *Nat. Chem.*, 2009, **1**, 552–556.
- 11 M. Oezaslan, M. Heggen and P. Strasser, *J. Am. Chem. Soc.*, 2011, **134**, 514–524.
- 12 I. Dumitrescu and R. M. Crooks, *Proc. Natl. Acad. Sci. U. S. A.*, 2012, **109**, 11493–11497.
- 13 L. Gan, M. Heggen, S. Rudi and P. Strasser, *Nano Lett.*, 2012, **12**, 5423–5430.
- 14 L. Gan, C. Cui, S. Rudi and P. Strasser, *Top. Catal.*, 2014, **57**, 236–244.
- 15 D. Wang, H. L. Xin, R. Hovden, H. Wang, Y. Yu, D. A. Muller, F. J. DiSalvo and H. D. Abruna, *Nat. Mater.*, 2013, **12**, 81–87.
- 16 J. Kibsgaard, Y. Gorlin, Z. Chen and T. F. Jaramillo, *J. Am. Chem. Soc.*, 2012, **134**, 7758–7765.
- 17 C. Chen, Y. Kang, Z. Huo, Z. Zhu, W. Huang, H. L. Xin, J. D. Snyder, D. Li, J. A. Herron, M. Mavrikakis, M. Chi, K. L. More, Y. Li, N. M. Markovic, G. A. Somorjai, P. Yang and V. R. Stamenkovic, *Science*, 2014, **343**, 1339–1343.
- 18 D. F. van der Vliet, C. Wang, D. Tripkovic, D. Strmcnik, X. F. Zhang, M. K. Debe, R. T. Atanasoski, N. M. Markovic and V. R. Stamenkovic, *Nat. Mater.*, 2012, **11**, 1051–1058.
- 19 Y. Chen, J. Wang, X. Meng, Y. Zhong, R. Li, X. Sun, S. Ye and S. Knights, *J. Power Sources*, 2013, **238**, 144–149.
- 20 V. Tripković, F. Abild-Pedersen, F. Studt, I. Cerri, T. Nagami, T. Bligaard and J. Rossmeisl, *ChemCatChem*, 2012, **4**, 228–235.
- 21 R. Kou, Y. Shao, D. Mei, Z. Nie, D. Wang, C. Wang, V. V. Viswanathan, S. Park, I. A. Aksay, Y. Lin, Y. Wang and J. Liu, *J. Am. Chem. Soc.*, 2011, **133**, 2541–2547.
- 22 B. Winther-Jensen, O. Winther-Jensen, M. Forsyth and D. R. MacFarlane, *Science*, 2008, **321**, 671–674.
- 23 G. Wu and P. Zelenay, *Acc. Chem. Res.*, 2013, **46**, 1878–1889.
- 24 G. Wu, K. L. More, C. M. Johnston and P. Zelenay, *Science*, 2011, **332**, 443–447.
- 25 M. Lefevre, E. Proietti, F. Jaouen and J.-P. Dodelet, *Science*, 2009, **324**, 71–74.
- 26 A. Brouzgou, S. Q. Song and P. Tsiakaras, *Appl. Catal., B*, 2012, **127**, 371–388.
- 27 M. Shao, *J. Power Sources*, 2011, **196**, 2433–2444.
- 28 Q. Li, R. Cao, J. Cho and G. Wu, *Adv. Energy Mater.*, 2014, **4**, 1301415.
- 29 D. S. Su and G. Sun, *Angew. Chem., Int. Ed.*, 2011, **50**, 11570–11572.
- 30 R. Bashyam and P. Zelenay, *Nature*, 2006, **443**, 63–66.
- 31 Y. Sha, T. H. Yu, B. V. Merinov and W. A. Goddard, *ACS Catal.*, 2014, **4**, 1189–1197.
- 32 L. Qu, Y. Liu, J.-B. Baek and L. Dai, *ACS Nano*, 2010, **4**, 1321–1326.
- 33 E. Biddinger, D. von Deak and U. Ozkan, *Top. Catal.*, 2009, **52**, 1566–1574.
- 34 P. H. Matter, L. Zhang and U. S. Ozkan, *J. Catal.*, 2006, **239**, 83–96.
- 35 P. H. Matter, E. Wang, M. Arias, E. J. Biddinger and U. S. Ozkan, *J. Mol. Catal. A: Chem.*, 2007, **264**, 73–81.
- 36 K. Gong, F. Du, Z. Xia, M. Durstock and L. Dai, *Science*, 2009, **323**, 760–764.
- 37 K. S. Novoselov, A. K. Geim, S. V. Morozov, D. Jiang, Y. Zhang, S. V. Dubonos, I. V. Grigorieva and A. A. Firsov, *Science*, 2004, **306**, 666–669.
- 38 A. K. Geim, *Science*, 2009, **324**, 1530–1534.
- 39 H. Liu, Y. Liu and D. Zhu, *J. Mater. Chem.*, 2011, **21**, 3335–3345.
- 40 T. Humberto, L. Ruitao, T. Mauricio and S. D. Mildred, *Rep. Prog. Phys.*, 2012, **75**, 062501.
- 41 R. Lv and M. Terrones, *Mater. Lett.*, 2012, **78**, 209–218.
- 42 C. H. Choi, H.-K. Lim, M. W. Chung, J. C. Park, H. Shin, H. Kim and S. I. Woo, *J. Am. Chem. Soc.*, 2014, **136**, 9070–9077.
- 43 C. Zhang, N. Mahmood, H. Yin, F. Liu and Y. Hou, *Adv. Mater.*, 2013, **25**, 4932–4937.
- 44 L. S. Panchakarla, K. S. Subrahmanyam, S. K. Saha, A. Govindaraj, H. R. Krishnamurthy, U. V. Waghmare and C. N. R. Rao, *Adv. Mater.*, 2009, **21**, 4726–4730.
- 45 B. Guo, Q. Liu, E. Chen, H. Zhu, L. Fang and J. R. Gong, *Nano Lett.*, 2010, **10**, 4975–4980.
- 46 N. Li, Z. Wang, K. Zhao, Z. Shi, Z. Gu and S. Xu, *Carbon*, 2010, **48**, 255–259.
- 47 Y.-C. Lin, C.-Y. Lin and P.-W. Chiu, *Appl. Phys. Lett.*, 2010, **96**, 133110.
- 48 D. Deng, X. Pan, L. Yu, Y. Cui, Y. Jiang, J. Qi, W.-X. Li, Q. Fu, X. Ma, Q. Xue, G. Sun and X. Bao, *Chem. Mater.*, 2011, **23**, 1188–1193.
- 49 L. Feng, Y. Chen and L. Chen, *ACS Nano*, 2011, **5**, 9611–9618.
- 50 D. Geng, Y. Chen, Y. Chen, Y. Li, R. Li, X. Sun, S. Ye and S. Knights, *Energy Environ. Sci.*, 2011, **4**, 760–764.
- 51 Z. Jin, J. Yao, C. Kittrell and J. M. Tour, *ACS Nano*, 2011, **5**, 4112–4117.
- 52 T. Lin, F. Huang, J. Liang and Y. Wang, *Energy Environ. Sci.*, 2011, **4**, 862–865.
- 53 Z.-H. Sheng, L. Shao, J.-J. Chen, W.-J. Bao, F.-B. Wang and X.-H. Xia, *ACS Nano*, 2011, **5**, 4350–4358.
- 54 Z. Yang, Z. Yao, G. Li, G. Fang, H. Nie, Z. Liu, X. Zhou, X. A. Chen and S. Huang, *ACS Nano*, 2011, **6**, 205–211.
- 55 D. Geng, Y. Hu, Y. Li, R. Li and X. Sun, *Electrochem. Commun.*, 2012, **22**, 65–68.

- 56 G. Hui, L. Zheng, S. Li, G. Wenhua, G. Wei, C. Lijie, R. Amrita, Q. Weijin, V. Robert and M. A. Pulickel, *Nanotechnology*, 2012, **23**, 275605.
- 57 J. Liang, Y. Jiao, M. Jaroniec and S. Z. Qiao, *Angew. Chem., Int. Ed.*, 2012, **51**, 11496–11500.
- 58 Z. Lin, M.-k. Song, Y. Ding, Y. Liu, M. Liu and C.-P. Wong, *Phys. Chem. Chem. Phys.*, 2012, **14**, 3381–3387.
- 59 Z. Lin, G. Waller, Y. Liu, M. Liu and C.-P. Wong, *Adv. Energy Mater.*, 2012, **2**, 884–888.
- 60 B. Shen, J. Chen, X. Yan and Q. Xue, *RSC Adv.*, 2012, **2**, 6761–6764.
- 61 L. Sun, L. Wang, C. Tian, T. Tan, Y. Xie, K. Shi, M. Li and H. Fu, *RSC Adv.*, 2012, **2**, 4498–4506.
- 62 S. Wang, L. Zhang, Z. Xia, A. Roy, D. W. Chang, J.-B. Baek and L. Dai, *Angew. Chem., Int. Ed.*, 2012, **51**, 4209–4212.
- 63 Z. Wen, X. Wang, S. Mao, Z. Bo, H. Kim, S. Cui, G. Lu, X. Feng and J. Chen, *Adv. Mater.*, 2012, **24**, 5610–5616.
- 64 T. Wu, H. Shen, L. Sun, B. Cheng, B. Liu and J. Shen, *New J. Chem.*, 2012, **36**, 1385–1391.
- 65 S. Yang, L. Zhi, K. Tang, X. Feng, J. Maier and K. Müllen, *Adv. Funct. Mater.*, 2012, **22**, 3634–3640.
- 66 S.-Y. Yang, K.-H. Chang, Y.-L. Huang, Y.-F. Lee, H.-W. Tien, S.-M. Li, Y.-H. Lee, C.-H. Liu, C.-C. M. Ma and C.-C. Hu, *Electrochem. Commun.*, 2012, **14**, 39–42.
- 67 Z. Yao, H. Nie, Z. Yang, X. Zhou, Z. Liu and S. Huang, *Chem. Commun.*, 2012, **48**, 1027–1029.
- 68 L. Chen, X. Cui, Y. Wang, M. Wang, R. Qiu, Z. shu, L. Zhang, Z. Hua, F. Cui, C. Wei and J. Shi, *Dalton Trans.*, 2014, **43**, 3420–3423.
- 69 C. H. Choi, M. W. Chung, Y. J. Jun and S. I. Woo, *RSC Adv.*, 2013, **3**, 12417–12422.
- 70 C. H. Choi, M. W. Chung, H. C. Kwon, S. H. Park and S. I. Woo, *J. Mater. Chem. A*, 2013, **1**, 3694–3699.
- 71 H.-L. Guo, P. Su, X. Kang and S.-K. Ning, *J. Mater. Chem. A*, 2013, **1**, 2248–2255.
- 72 R. Li, Z. Wei, X. Gou and W. Xu, *RSC Adv.*, 2013, **3**, 9978–9984.
- 73 Z.-J. Lu, S.-J. Bao, Y.-T. Gou, C.-J. Cai, C.-C. Ji, M.-W. Xu, J. Song and R. Wang, *RSC Adv.*, 2013, **3**, 3990–3995.
- 74 H. L. Poh, P. Šimek, Z. Sofer and M. Pumera, *ACS Nano*, 2013, **7**, 5262–5272.
- 75 Y. Su, Y. Zhang, X. Zhuang, S. Li, D. Wu, F. Zhang and X. Feng, *Carbon*, 2013, **62**, 296–301.
- 76 J. Wu, D. Zhang, Y. Wang and B. Hou, *J. Power Sources*, 2013, **227**, 185–190.
- 77 J. Xu, G. Dong, C. Jin, M. Huang and L. Guan, *ChemSusChem*, 2013, **6**, 493–499.
- 78 C. Zhang, R. Hao, H. Liao and Y. Hou, *Nano Energy*, 2013, **2**, 88–97.
- 79 B. Zheng, J. Wang, F.-B. Wang and X.-H. Xia, *Electrochem. Commun.*, 2013, **28**, 24–26.
- 80 Y. Zheng, Y. Jiao, L. Ge, M. Jaroniec and S. Z. Qiao, *Angew. Chem., Int. Ed.*, 2013, **52**, 3110–3116.
- 81 J.-e. Park, Y. J. Jang, Y. J. Kim, M.-s. Song, S. Yoon, D. H. Kim and S.-J. Kim, *Phys. Chem. Chem. Phys.*, 2014, **16**, 103–109.
- 82 M. Bacon, S. J. Bradley and T. Nann, *Part. Part. Syst. Charact.*, 2014, **31**, 415–428.
- 83 I.-Y. Jeon, H.-J. Choi, M. Choi, J.-M. Seo, S.-M. Jung, M.-J. Kim, S. Zhang, L. Zhang, Z. Xia, L. Dai, N. Park and J.-B. Baek, *Sci. Rep.*, 2013, **3**, 1810.
- 84 Y. Zhao, L. Yang, S. Chen, X. Wang, Y. Ma, Q. Wu, Y. Jiang, W. Qian and Z. Hu, *J. Am. Chem. Soc.*, 2013, **135**, 1201–1204.
- 85 L. Ferrighi, M. Datteo and C. Di Valentin, *J. Phys. Chem. C*, 2013, **118**, 223–230.
- 86 T. Ikeda, M. Boero, S.-F. Huang, K. Terakura, M. Oshima, J.-I. Ozaki and S. Miyata, *J. Phys. Chem. C*, 2010, **114**, 8933–8937.
- 87 L. Yu, X. Pan, X. Cao, P. Hu and X. Bao, *J. Catal.*, 2011, **282**, 183–190.
- 88 L. Zhang and Z. Xia, *J. Phys. Chem. C*, 2011, **115**, 11170–11176.
- 89 H. Tominaga, W. Ikeda and M. Nagai, *Phys. Chem. Chem. Phys.*, 2011, **13**, 2659–2662.
- 90 H. Kim, K. Lee, S. I. Woo and Y. Jung, *Phys. Chem. Chem. Phys.*, 2011, **13**, 17505–17510.
- 91 X. Bao, X. Nie, D. von Deak, E. Biddinger, W. Luo, A. Asthagiri, U. Ozkan and C. Hadad, *Top. Catal.*, 2013, **56**, 1623–1633.
- 92 Y. Okamoto, *Appl. Surf. Sci.*, 2009, **256**, 335–341.
- 93 S.-F. Huang, K. Terakura, T. Ozaki, T. Ikeda, M. Boero, M. Oshima, J.-I. Ozaki and S. Miyata, *Phys. Rev. B: Condens. Matter Mater. Phys.*, 2009, **80**, 235410.
- 94 D. W. Boukhvalov and Y.-W. Son, *Nanoscale*, 2012, **4**, 417–420.
- 95 L. Zhang, J. Niu, L. Dai and Z. Xia, *Langmuir*, 2012, **28**, 7542–7550.
- 96 K. Hisayoshi, T. Nakazono, M. Soichi, M. Toshiko, T. Nobuyuki and Y. Tokio, *IOP Conf. Ser.: Mater. Sci. Eng.*, 2011, **18**, 122010.
- 97 Y. Feng, F. Li, Z. Hu, X. Luo, L. Zhang, X.-F. Zhou, H.-T. Wang, J.-J. Xu and E. G. Wang, *Phys. Rev. B: Condens. Matter Mater. Phys.*, 2012, **85**, 155454.
- 98 L. Zhang, J. Niu, M. Li and Z. Xia, *J. Phys. Chem. C*, 2014, **118**, 3545–3553.
- 99 J. Zhang, Z. Wang and Z. Zhu, *J. Mol. Model.*, 2013, **19**, 5515–5521.
- 100 X. Kong, Q. Chen and Z. Sun, *ChemPhysChem*, 2013, **14**, 514–519.
- 101 M. Kaukonen, A. V. Krasheninnikov, E. Kauppinen and R. M. Nieminen, *ACS Catal.*, 2012, **3**, 159–165.
- 102 V. V. Strelko, V. S. Kuts and P. A. Thrower, *Carbon*, 2000, **38**, 1499–1503.
- 103 X. Fan, W. T. Zheng and J.-L. Kuo, *RSC Adv.*, 2013, **3**, 5498–5505.
- 104 Z. Liu, H. Nie, Z. Yang, J. Zhang, Z. Jin, Y. Lu, Z. Xiao and S. Huang, *Nanoscale*, 2013, **5**, 3283–3288.
- 105 C. H. Choi, M. W. Chung, S. H. Park and S. I. Woo, *Phys. Chem. Chem. Phys.*, 2013, **15**, 1802–1805.
- 106 Z. Lin, G. H. Waller, Y. Liu, M. Liu and C.-P. Wong, *Nano Energy*, 2013, **2**, 241–248.
- 107 Y. Xue, D. Yu, L. Dai, R. Wang, D. Li, A. Roy, F. Lu, H. Chen, Y. Liu and J. Qu, *Phys. Chem. Chem. Phys.*, 2013, **15**, 12220–12226.

- 108 Z.-H. Sheng, H.-L. Gao, W.-J. Bao, F.-B. Wang and X.-H. Xia, *J. Mater. Chem.*, 2012, **22**, 390–395.
- 109 L. Song, Z. Liu, A. L. M. Reddy, N. T. Narayanan, J. Taha-Tijerina, J. Peng, G. Gao, J. Lou, R. Vajtai and P. M. Ajayan, *Adv. Mater.*, 2012, **24**, 4878–4895.
- 110 D. S. Su, J. Zhang, B. Frank, A. Thomas, X. Wang, J. Paraknowitsch and R. Schlögl, *ChemSusChem*, 2010, **3**, 169–180.
- 111 Y. Zheng, Y. Jiao, M. Jaroniec, Y. Jin and S. Z. Qiao, *Small*, 2012, **8**, 3550–3566.
- 112 Z. Yang, H. Nie, X. A. Chen, X. Chen and S. Huang, *J. Power Sources*, 2013, **236**, 238–249.
- 113 X. Zhou, J. Qiao, L. Yang and J. Zhang, *Adv. Energy Mater.*, 2014, **4**, 1301523.
- 114 D. S. Su and G. Centi, *J. Energy Chem.*, 2013, **22**, 151–173.
- 115 D.-W. Wang and D. Su, *Energy Environ. Sci.*, 2014, **7**, 576–591.
- 116 M. Zhang and L. Dai, *Nano Energy*, 2012, **1**, 514–517.
- 117 D. Yu, E. Nagelli, F. Du and L. Dai, *J. Phys. Chem. Lett.*, 2010, **1**, 2165–2173.
- 118 C. Su and K. P. Loh, *Acc. Chem. Res.*, 2012, **46**, 2275–2285.
- 119 D. Haag and H. Kung, *Top. Catal.*, 2014, **57**, 762–773.
- 120 B. Xia, Y. Yan, X. Wang and X. W. Lou, *Mater. Horiz.*, 2014, **1**, 379–399.
- 121 X. Wang, G. Sun, P. Routh, D.-H. Kim, W. Huang and P. Chen, *Chem. Soc. Rev.*, 2014, **43**, 7067–7098.
- 122 K. N. Wood, R. O'Hayre and S. Pylypenko, *Energy Environ. Sci.*, 2014, **7**, 1212–1249.
- 123 H. Wang, T. Maiyalagan and X. Wang, *ACS Catal.*, 2012, **2**, 781–794.
- 124 C. Zhu and S. Dong, *Nanoscale*, 2013, **5**, 1753–1767.
- 125 N. Mahmood, C. Zhang, H. Yin and Y. Hou, *J. Mater. Chem. A*, 2014, **2**, 15–32.
- 126 X.-K. Kong, C.-L. Chen and Q.-W. Chen, *Chem. Soc. Rev.*, 2014, **43**, 2841–2857.
- 127 M. Liu, R. Zhang and W. Chen, *Chem. Rev.*, 2014, **114**, 5117–5160.
- 128 F. López-Uriás, R. Lv, H. Terrones and M. Terrones, in *Graphene Chemistry*, John Wiley & Sons, Ltd, 2013, ch. 9, pp. 183–207.
- 129 E. Yeager, *Electrochim. Acta*, 1984, **29**, 1527–1537.
- 130 N. Ramaswamy and S. Mukerjee, *Adv. Phys. Chem.*, 2012, **2012**, 17.
- 131 B. B. Blizanac, P. N. Ross and N. M. Markovic, *Electrochim. Acta*, 2007, **52**, 2264–2271.
- 132 V. V. Strelko, N. T. Kartel, I. N. Dukhno, V. S. Kuts, R. B. Clarkson and B. M. Odintsov, *Surf. Sci.*, 2004, **548**, 281–290.
- 133 N. M. Marković and P. N. Ross Jr, *Surf. Sci. Rep.*, 2002, **45**, 117–229.
- 134 X. Chen, D. Xia, Z. Shi and J. Zhang, in *Electrocatalysis in Fuel Cells*, ed. M. Shao, Springer, London, 2013, vol. 9, ch. 11, pp. 339–373.
- 135 C. Song and J. Zhang, in *PEM Fuel Cell Electrocatalysts and Catalyst Layers*, ed. J. Zhang, Springer, London, 2008, ch. 2, pp. 89–134.
- 136 W. E. Mustain and J. Prakash, *J. Electrochem. Soc.*, 2007, **154**, A668–A676.
- 137 D. B. Sepa, M. V. Vojnovic and A. Damjanovic, *Electrochim. Acta*, 1980, **25**, 1491–1496.
- 138 S. Dou, A. Shen, L. Tao and S. Wang, *Chem. Commun.*, 2014, **50**, 10672–10675.
- 139 The U. S. Department of Energy (DOE), http://energy.gov/sites/prod/files/2014/03/f12/fuel_cells.pdf.
- 140 C. He, Z. Li, M. Cai, M. Cai, J.-Q. Wang, Z. Tian, X. Zhang and P. K. Shen, *J. Mater. Chem. A*, 2013, **1**, 1401–1406.
- 141 Y. Shao, S. Zhang, M. H. Engelhard, G. Li, G. Shao, Y. Wang, J. Liu, I. A. Aksay and Y. Lin, *J. Mater. Chem.*, 2010, **20**, 7491–7496.
- 142 Z. Luo, S. Lim, Z. Tian, J. Shang, L. Lai, B. MacDonald, C. Fu, Z. Shen, T. Yu and J. Lin, *J. Mater. Chem.*, 2011, **21**, 8038–8044.
- 143 Y. Zhang, J. Ge, L. Wang, D. Wang, F. Ding, X. Tao and W. Chen, *Sci. Rep.*, 2013, **3**, 2771.
- 144 J. Li, X.-B. Wang, J. Yang, X.-Y. Yang and L. Wan, *Chem. J. Chin. Univ.*, 2013, **34**, 800–805.
- 145 Y. Ito, C. Christodoulou, M. V. Nardi, N. Koch, H. Sachdev and K. Müllen, *ACS Nano*, 2014, **8**, 3337–3346.
- 146 C. Zhang, L. Fu, N. Liu, M. Liu, Y. Wang and Z. Liu, *Adv. Mater.*, 2011, **23**, 1020–1024.
- 147 C. Bronner, S. Strelau, M. Gille, F. Brausse, A. Haase, S. Hecht and P. Tegeder, *Angew. Chem., Int. Ed.*, 2013, **52**, 4422–4425.
- 148 K. T. Kim, J. W. Lee and W. H. Jo, *Macromol. Chem. Phys.*, 2013, **214**, 2768–2773.
- 149 T. H. Vo, M. Shekhiriev, D. A. Kunkel, F. Orange, M. J. F. Guinel, A. Enders and A. Sinitskii, *Chem. Commun.*, 2014, **50**, 4172–4174.
- 150 H. M. Jeong, J. W. Lee, W. H. Shin, Y. J. Choi, H. J. Shin, J. K. Kang and J. W. Choi, *Nano Lett.*, 2011, **11**, 2472–2477.
- 151 Z. Lin, G. H. Waller, Y. Liu, M. Liu and C.-P. Wong, *Carbon*, 2013, **53**, 130–136.
- 152 K. R. Lee, K. U. Lee, J. W. Lee, B. T. Ahn and S. I. Woo, *Electrochem. Commun.*, 2010, **12**, 1052–1055.
- 153 D. Yu, L. Wei, W. Jiang, H. Wang, B. Sun, Q. Zhang, K. Goh, R. Si and Y. Chen, *Nanoscale*, 2013, **5**, 3457–3464.
- 154 L. Lai, J. R. Potts, D. Zhan, L. Wang, C. K. Poh, C. Tang, H. Gong, Z. Shen, J. Lin and R. S. Ruoff, *Energy Environ. Sci.*, 2012, **5**, 7936–7942.
- 155 C. L. Liu, C.-C. Hu, S.-H. Wu and T.-H. Wu, *J. Electrochem. Soc.*, 2013, **160**, H547–H552.
- 156 S. Yasuda, L. Yu, J. Kim and K. Murakoshi, *Chem. Commun.*, 2013, **49**, 9627–9629.
- 157 Y. Jiao, Y. Zheng, M. Jaroniec and S. Z. Qiao, *J. Am. Chem. Soc.*, 2014, **136**, 4394–4403.
- 158 X. Cao, Z. Yin and H. Zhang, *Energy Environ. Sci.*, 2014, **7**, 1850–1865.
- 159 X. Bo, C. Han, Y. Zhang and L. Guo, *ACS Appl. Mater. Interfaces*, 2014, **6**, 3030–3037.
- 160 L. Jiang and Z. Fan, *Nanoscale*, 2014, **6**, 1922–1945.
- 161 W. Yuan, J. Chen and G. Shi, *Mater. Today*, 2014, **17**, 77–85.
- 162 R. Paola, H. Anming and C. Giuseppe, *Nano-Micro Lett.*, 2013, **5**, 260–273.
- 163 P. Xu, J. Yang, K. Wang, Z. Zhou and P. Shen, *Chin. Sci. Bull.*, 2012, **57**, 2948–2955.

- 164 Z. Zhang, J. Zhang, N. Chen and L. Qu, *Energy Environ. Sci.*, 2012, **5**, 8869–8890.
- 165 Y. Li, Y. Zhao, H. Cheng, Y. Hu, G. Shi, L. Dai and L. Qu, *J. Am. Chem. Soc.*, 2012, **134**, 15–18.
- 166 P. Wang, Z. Wang, L. Jia and Z. Xiao, *Phys. Chem. Chem. Phys.*, 2009, **11**, 2730–2740.
- 167 C.-M. Chen, Q. Zhang, C.-H. Huang, X.-C. Zhao, B.-S. Zhang, Q.-Q. Kong, M.-Z. Wang, Y.-G. Yang, R. Cai and D. S. Su, *Chem. Commun.*, 2012, **48**, 7149–7151.
- 168 X. Wang, Y. Zhang, C. Zhi, X. Wang, D. Tang, Y. Xu, Q. Weng, X. Jiang, M. Mitome, D. Golberg and Y. Bando, *Nat. Commun.*, 2013, **4**, 2905.
- 169 Z.-L. Wang, D. Xu, H.-G. Wang, Z. Wu and X.-B. Zhang, *ACS Nano*, 2013, **7**, 2422–2430.
- 170 D. Deng, L. Yu, X. Pan, S. Wang, X. Chen, P. Hu, L. Sun and X. Bao, *Chem. Commun.*, 2011, **47**, 10016–10018.
- 171 A. Shen, Y. Zou, Q. Wang, R. A. Dryfe, X. Huang, S. Dou, L. Dai and S. Wang, *Angew. Chem., Int. Ed.*, 2014, **53**, 10804–10808.
- 172 X. Fu, J. Jin, Y. Liu, Z. Wei, F. Pan and J. Zhang, *ACS Appl. Mater. Interfaces*, 2014, **6**, 3930–3936.
- 173 Q. Li, S. Zhang, L. Dai and L.-S. Li, *J. Am. Chem. Soc.*, 2012, **134**, 18932–18935.
- 174 Y. Liu and P. Wu, *ACS Appl. Mater. Interfaces*, 2013, **5**, 3362–3369.
- 175 H. Niwa, K. Horiba, Y. Harada, M. Oshima, T. Ikeda, K. Terakura, J.-I. Ozaki and S. Miyata, *J. Power Sources*, 2009, **187**, 93–97.
- 176 X. Wang, Z. Hou, T. Ikeda, M. Oshima, M.-A. Kakimoto and K. Terakura, *J. Mater. Chem. A*, 2012, **117**, 579–589.
- 177 S. C. Ray, C. W. Pao, J. W. Chiou, H. M. Tsai, J. C. Jan, W. F. Pong, R. McCann, S. S. Roy, P. Papakonstantinou and J. A. McLaughlin, *J. Appl. Phys.*, 2005, **98**, 033708.
- 178 J. R. Pels, F. Kapteijn, J. A. Moulijn, Q. Zhu and K. M. Thomas, *Carbon*, 1995, **33**, 1641–1653.
- 179 J. C. Meyer, S. Kurasch, H. J. Park, V. Skakalova, D. Künzel, A. Groß, A. Chuvilin, G. Algara-Siller, S. Roth, T. Iwasaki, U. Starke, J. H. Smet and U. Kaiser, *Nat. Mater.*, 2011, **10**, 209–215.
- 180 L. Zhao, R. He, K. T. Rim, T. Schiros, K. S. Kim, H. Zhou, C. Gutiérrez, S. P. Chockalingam, C. J. Arguello, L. Pálková, D. Nordlund, M. S. Hybertsen, D. R. Reichman, T. F. Heinz, P. Kim, A. Pinczuk, G. W. Flynn and A. N. Pasupathy, *Science*, 2011, **333**, 999–1003.
- 181 H. Wang, Q. Wang, Y. Cheng, K. Li, Y. Yao, Q. Zhang, C. Dong, P. Wang, U. Schwingenschlögl, W. Yang and X. X. Zhang, *Nano Lett.*, 2011, **12**, 141–144.
- 182 L. Zhao, M. Levendorf, S. Goncher, T. Schiros, L. Pálková, A. Zabet-Khosousi, K. T. Rim, C. Gutiérrez, D. Nordlund, C. Jaye, M. Hybertsen, D. Reichman, G. W. Flynn, J. Park and A. N. Pasupathy, *Nano Lett.*, 2013, **13**, 4659–4665.
- 183 B. J. Schultz, C. J. Patridge, V. Lee, C. Jaye, P. S. Lysaght, C. Smith, J. Barnett, D. A. Fischer, D. Prendergast and S. Banerjee, *Nat. Commun.*, 2011, **2**, 372.
- 184 R. Lv, Q. Li, A. R. Botello-Méndez, T. Hayashi, B. Wang, A. Berkdemir, Q. Hao, A. L. Elías, R. Cruz-Silva, H. R. Gutiérrez, Y. A. Kim, H. Muramatsu, J. Zhu, M. Endo, H. Terrones, J.-C. Charlier, M. Pan and M. Terrones, *Sci. Rep.*, 2012, **2**, 586.
- 185 L. Wang, A. Ambrosi and M. Pumera, *Angew. Chem., Int. Ed.*, 2013, **52**, 13818–13821.
- 186 K. J. J. Mayrhofer, D. Strmcnik, B. B. Blizanac, V. Stamenkovic, M. Arenz and N. M. Markovic, *Electrochim. Acta*, 2008, **53**, 3181–3188.
- 187 U. A. Paulus, T. J. Schmidt, H. A. Gasteiger and R. J. Behm, *J. Electroanal. Chem.*, 2001, **495**, 134–145.